

---

# Attention Projection Mixing and Exogenous Anchors

---

Jonathan Su

## Abstract

Transformers that reuse early-layer attention projections as residuals face a fundamental tension: the first layer must simultaneously serve as a stable reference for all deeper layers and as an effective computational block. To resolve this, we propose ExoFormer, which learns *dedicated exogenous anchor projections* outside the sequential layer stack, decoupling the anchor role from computational refinement. Through a unified normalized mixing framework (studying different coefficient granularities: elementwise, headwise, scalar) across all attention pathways (queries, keys, values, and gate logits), ExoFormer variants consistently outperform their internal-anchor counterparts. Moreover, the dynamic variant achieves a 2.13-point increase in downstream accuracy over the baseline and demonstrates superior data efficiency, matching baseline validation loss with  $1.84 \times$  fewer tokens. ExoFormer also achieves a  $2 \times$  reduction in attention sink compared to standard Gated Attention. Paradoxically, all ExoFormer variants exhibit signs of representation collapse. We explain this via an *Offloading Hypothesis*: external anchors preserve essential token identity, allowing layers to specialize exclusively in computational refinement. We release codes and models to facilitate future research.<sup>1</sup>

## 1 Introduction

The Transformer architecture (Vaswani et al., 2017) has become the foundation for modern large language models (LLMs) and a wide array of sequential and contextual tasks. A core component of its success is the multi-head self-attention mechanism, which enables dynamic, context-dependent interactions across sequences. However, as models scale in depth to capture more complex abstractions, ensuring stable and efficient training alongside effective information propagation remains a challenge.

A primary technique for stabilizing deep networks is the use of residual connections. In Transformers, a layer’s input is added to its output, preserving a pathway for gradients and early-layer information. Despite this, studies show that token-level information can become diluted in deeper layers, a phenomenon linked to over-smoothing (Shi et al., 2022; Zhou et al., 2021). This has spurred interest in more direct mechanisms for preserving early representations.

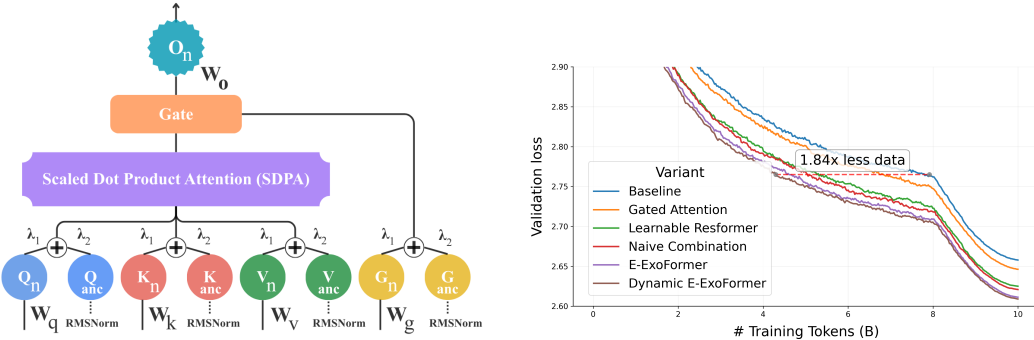
However, existing solutions largely operate in isolation and leave key questions unanswered. ResFormer (Zhou et al., 2025) focuses solely on residualizing *values*, leaving the potential reuse of other attention components—queries, keys, and gating logits—unexplored.

We first develop a unified framework for cross-layer mixing across all attention pathways: queries, keys, values, and gate logits. A key insight is that applying RMSNorm to the residual sources before mixing resolves distributional mismatch, enabling stable and beneficial reuse. The internal-anchor version, which we term NuResFormer (Normalized **u**nified), serves as a comparative foundation.

Analyzing architectures that reuse first-layer projections reveals a fundamental tension. The first layer is forced to serve two roles: (1) as a stable, reusable anchor for all deeper layers and (2) as

---

<sup>1</sup><https://github.com/jon123boss/ExoFormer>



(a) For **NuResFormer**, the anchor components are sourced from the first layer. For **ExoFormer**, they are provided by dedicated exogenous projections. All residualized sources are RMSNormed before being mixed with the current layer’s projections, and the scaled dot product attention (SDPA) output is gated.

(b) Training curves showing validation loss across steps. All models have similar parameter counts (453M–454M) except ExoFormer, which uses a dedicated exogenous anchor and has 457M parameters. ‘Naive Combination’ refers to the unmodified addition of Gated Attention and ResFormer.

Figure 1: Overview of the proposed architectures and their training performance.

an effective computational block for progressive feature transformation. This forced coexistence inherently limits effectiveness in both roles.

Our primary contribution is **ExoFormer**, which resolves this tension by learning a set of *dedicated exogenous anchor projections* outside the sequential layer stack. This decoupling proves consistently beneficial: every ExoFormer variant outperforms its corresponding NuResFormer counterpart in perplexity while remaining competitive in downstream accuracy despite no increase in width or depth, with the dynamic variant achieving the best results. Furthermore, ExoFormer exhibits a paradoxical combination of high performance and signs of representation collapse. We explain this via an *Offloading Hypothesis*: the external anchor assumes the role of preserving token identity, allowing the sequential layers to specialize almost exclusively in refinement.

## 2 Related Work

**Value Residuals and Gated Attention.** Most directly relevant are ResFormer and Gated Attention. Zhou et al. (2025) introduced *Value Residual Learning* (ResFormer), which adds a residual connection from the first layer’s value vectors ( $V_1$ ) to the value projections of all subsequent layers. This simple yet effective method was shown to greatly improve model performance and data efficiency, highlighting the benefit of explicitly reusing early content representations. However, preliminary attempts to residualize queries and keys were found to be unstable. Concurrently, gated attention mechanisms have been explored to introduce dynamic, input-dependent modulation to the attention output, improving expressiveness and training stability (Qiu et al., 2025). Our work generalizes residual learning beyond values and integrates it with gating via normalized mixing.

**Cross-layer communication and residual mixing.** Recent work has sought to improve cross-layer information flow in Transformers beyond simple residual connections. Zhu et al. (2025) proposed Hyper-Connections that expand residual stream width. More recently, Xie et al. (2026) introduced Manifold-Constrained Hyper-Connections (mHC), restoring an identity-like signal-preservation property to hyper-connected architecture.

Most closely related to our work—though orthogonal in direction—is **MUDDFormer** (Xiao et al., 2025), which proposes Multiway Dynamic Dense (MUDD) connections. MUDDFormer decouples the input to each Transformer block into four streams (query, key, value, residual) and dynamically aggregates outputs from *all* preceding layers using context-specific weights generated by a small MLP.

While both MUDDFormer and our work focus on enhancing the attention pathways, they operate at different levels and can coexist. MUDDFormer primarily addresses the *input* to the QKV pro-

jections. In contrast, our unified mixing framework focuses on *mixing* the projected QKV tensors themselves. Our approach can be seen as a form of residual blending *after* projection, whereas MUDDFormer enriches the input *before* projection.

### 3 Methodology

#### 3.1 Preliminaries and Notation

For the  $n$ -th Transformer layer, let  $H_{n-1} \in \mathbb{R}^{T \times d_{\text{model}}}$  be the input hidden states (after pre-normalization), where  $T$  is the sequence length and  $d_{\text{model}}$  is the model width. We use  $h$  attention heads and per-head dimension  $d_k$  such that  $d_{\text{model}} = h d_k$ . We denote the projected queries, keys, values, and gate logits as  $Q_n, K_n, V_n, G_n$ . Let  $\text{RMSNorm}(\cdot)$  denote per-token RMS normalization applied independently to each attention head (with learnable gain).

**Granularity of learned coefficients.** We consider three coefficient granularities throughout for  $\lambda$ :

- **Scalar (S):** a single coefficient shared across all channels.
- **Headwise (H):** one coefficient per head, broadcast across the head dimension  $d_k$ .
- **Elementwise (E):** one coefficient per channel.

#### 3.2 Multi-Head Attention

We describe attention as a sequence of stages, with two standard enhancements integrated implicitly: rotary position embeddings (RoPE) (Su et al., 2023) and query/key normalization (QKNorm) (Henry et al., 2020). For simplicity, the multi-head mechanism is presented using unified tensors with an implicit head dimension.

**Stage 1: QKV Linear Projections.** Given  $H_{n-1} \in \mathbb{R}^{T \times d_{\text{model}}}$ , we compute the projected tensors:

$$Q_n = H_{n-1} W_n^Q, \quad K_n = H_{n-1} W_n^K, \quad V_n = H_{n-1} W_n^V, \quad (1)$$

where  $W_n^Q, W_n^K, W_n^V \in \mathbb{R}^{d_{\text{model}} \times d_{\text{model}}}$ . The resulting  $Q_n, K_n, V_n$  are structured to contain  $h$  heads implicitly.

**Stage 2: Scaled Dot-Product Attention (SDPA).** Attention is computed per head, which is represented here as a single operation:

$$A_n = \text{softmax} \left( \frac{Q_n K_n^\top}{\sqrt{d_k}} \right) \in \mathbb{R}^{T \times T}, \quad U_n = A_n V_n \in \mathbb{R}^{T \times d_{\text{model}}}, \quad (2)$$

where the operations encompass the independent computations across  $h$  heads.

**Stage 3: Final Output Projection.** The output of the attention computation is projected:

$$O_n = U_n W_n^O, \quad W_n^O \in \mathbb{R}^{d_{\text{model}} \times d_{\text{model}}}. \quad (3)$$

In NuResFormer/ExoFormer, the above stages use mixed tensors  $\widehat{Q}_n, \widehat{K}_n, \widehat{V}_n$  from Eq. (10). Note that while heads are not shown explicitly in this formulation, the practical implementation follows the standard multi-head mechanism.

#### 3.3 Gated Attention

We adopt the elementwise head-specific multiplicative gating formulation as described by Qiu et al. (2025). The general form is:

$$Y' = g(Y, X, W_\theta, \sigma) = Y \odot \sigma(XW_\theta), \quad (4)$$

where  $Y$  is the feature tensor to be modulated,  $X$  is the input used to compute the gating scores,  $W_\theta$  are learnable parameters,  $\sigma$  is an activation function (sigmoid unless stated otherwise), and  $\odot$  denotes elementwise multiplication.

In our attention block, we apply gating to the concatenated multi-head output (i.e., after Stage 4 and before Stage 5). Let  $G_n \in \mathbb{R}^{T \times (hd_k)}$  denote the gate logits, computed from  $H_{n-1}$ :

$$G_n = H_{n-1}W_n^G, \quad W_n^G \in \mathbb{R}^{d_{\text{model}} \times (hd_k)}. \quad (5)$$

Then the gated attention output is

$$\tilde{U}_n = U_n \odot \sigma(G_n), \quad O_n = \tilde{U}_n W_n^O. \quad (6)$$

**Normalization placement.** We note that in ablations, using post-norm instead of pre-norm substantially degraded gated attention performance.

### 3.4 Unified Mixing Formulation

We now present a general framework for mixing. The core idea is to enrich each layer’s attention pathways with a set of persistent *anchor projections*  $\{Q_{\text{anc}}, K_{\text{anc}}, V_{\text{anc}}, G_{\text{anc}}\}$  that are reused, via learnable mixing, across all layers.

**Current-layer projections.** For layer  $n$  with input  $H_{n-1}$ , we compute the standard projections:

$$Q_n = H_{n-1}W_n^Q, \quad K_n = H_{n-1}W_n^K, \quad V_n = H_{n-1}W_n^V, \quad G_n = H_{n-1}W_n^G. \quad (7)$$

**Anchor projections.** The anchor projections are a fixed set of tensors defined once for the entire model. In our work, we explore two instantiations:

- **NuResFormer:** The anchors are the projections from the very first attention layer. That is,

$$Q_{\text{anc}} = Q_1, \quad K_{\text{anc}} = K_1, \quad V_{\text{anc}} = V_1, \quad G_{\text{anc}} = G_1, \quad (8)$$

- **ExoFormer:** The anchors are produced by a dedicated, external projection module on the input embeddings:

$$Q_{\text{anc}} = H_0W_{\text{anc}}^Q, \quad K_{\text{anc}} = H_0W_{\text{anc}}^K, \quad V_{\text{anc}} = H_0W_{\text{anc}}^V, \quad G_{\text{anc}} = H_0W_{\text{anc}}^G, \quad (9)$$

with independent weight matrices  $W_{\text{anc}}^Q, W_{\text{anc}}^K, W_{\text{anc}}^V, W_{\text{anc}}^G$ .

**Mixing with normalized sources.** For each component  $S \in \{Q, K, V, G\}$ , we mix the anchor projection with the current-layer projection using learned coefficients. To stabilize the mixture, we apply RMS normalization to the anchor source before scaling:

$$\hat{S}_n = \lambda_{n,1}^S \odot \text{RMSNorm}(S_{\text{anc}}) + \lambda_{n,2}^S \odot S_n, \quad \forall S \in \{Q, K, V, G\}, \quad (10)$$

where  $\lambda_{n,1}^S, \lambda_{n,2}^S$  are coefficient tensors of the chosen granularity (scalar, headwise, or elementwise). All  $\lambda$  parameters are initialized to 0.5 and are learnable.

We apply QKNorm and RoPE to the mixed queries and keys,  $\hat{Q}_n$  and  $\hat{K}_n$ . We then compute the scaled dot-product attention per head using the mixed projections  $\hat{Q}_n, \hat{K}_n, \hat{V}_n$ , apply the gating operation using  $\hat{G}_n$ , and finally pass the result to the output projection.

### 3.5 First Layer Tension and ExoFormer

Cross-layer residual reuse makes early information available at every depth. This is powerful, but it implicitly forces the first layer to satisfy two pressures:

1. **Reusable anchor:** produce a broadly useful reference representation that remains valuable throughout depth.
2. **Progressive computation:** produce features that are easy for downstream layers to transform into increasingly task-relevant abstractions.

While these roles appear misaligned—universal anchors favor invariance, while progressive computation necessitates change—they can theoretically coexist because it is an *optional pathway* modulated by learned mixing coefficients  $(\lambda_{n,1}, \lambda_{n,2})$ . However, this forced coexistence compels the first layer to make compromises, inherently limiting its effectiveness in both roles.

We explored strategies to decouple the “anchor” role from the first attention layer. Our most successful approach, termed **ExoFormer** (where “Exo” signifies an external, outside-the-system anchor), instantiates the general framework of Section 3.4 with the dedicated exogenous projections of Eq. (9).

This decoupling proves beneficial: in our experiments, every ExoFormer variant outperformed its corresponding NuResFormer counterpart in perplexity, despite adding only four additional projection matrices with no change to depth or width. The result confirms that separating the reusable-anchor task from the progressive-computation task allows each component to specialize, leading to better downstream performance.

### 3.6 Dynamic Mixing (DM) Module

Building upon the unified formulation, we take inspiration from MUDDFormer’s Depth-wise Aggregate (DA) module (Xiao et al., 2025) and introduce a dynamic variant where the learnable parameters are modulated by context-dependent scaling factors computed from the layer input  $H_{n-1}$  using a small MLP. This allows the model to adapt its mixing strategy based on the specific context. It is possible to combine both modules (DA and DM) for increased efficiency since they share the same structure.

**Dynamic Coefficient Generation.** For each layer  $n$ , we compute modulation scalars from its input  $H_{n-1}$  (pre-normalized) using a two-layer MLP with GELU activation and sigmoid output:

$$\mathcal{DM}_n(H_{n-1}) = \sigma \left( \text{GELU}(H_{n-1} W_{n,1}^{\text{DM}}) W_{n,2}^{\text{DM}} + b_n^{\text{DM}} \right) \quad (11)$$

The trainable parameters for the Dynamic Mixing module at layer  $n$  are:

$$\theta_n^{\text{DM}} = \{W_{n,1}^{\text{DM}} \in \mathbb{R}^{d_{\text{model}} \times 16}, W_{n,2}^{\text{DM}} \in \mathbb{R}^{16 \times 8}, b_n^{\text{DM}} \in \mathbb{R}^8\}$$

The output dimension of this module is 8, corresponding to the dynamic scaling factors:

$$\{\gamma_{n,1}^Q, \gamma_{n,2}^Q, \gamma_{n,1}^K, \gamma_{n,2}^K, \gamma_{n,1}^V, \gamma_{n,2}^V, \gamma_{n,1}^G, \gamma_{n,2}^G\}$$

The output layer weights  $W_{n,2}^{\text{DM}}$  and bias  $b_n^{\text{DM}}$  are zero-initialized, ensuring that initial sigmoid outputs are 0.5. Consequently, the base  $\lambda$  parameters must be initialized at 1.0 to achieve effective identity mixing at initialization.

**Modulated Mixing.** For each component  $S \in \{Q, K, V, G\}$ :

$$\widehat{S}_n = (\lambda_{n,1}^S \odot \gamma_{n,1}^S) \odot \text{RMSNorm}(S_{\text{anc}}) + (\lambda_{n,2}^S \odot \gamma_{n,2}^S) \odot S_n \quad (12)$$

where  $\gamma_{n,i}^S$  are broadcast appropriately based on the residual granularity (elementwise, headwise, or scalar), and  $\lambda_{n,i}^S$  are the learnable base parameters.

## 4 Experiments

### 4.1 Experimental Setups

**Training Details** All models use a pre-normalized modern Transformer architecture with SwiGLU activations (Shazeer, 2020), QKNorm (Henry et al., 2020), and rotary position embeddings (Su et al., 2023). We follow prior work by initializing projection and classification layers to zero (Yang et al., 2022), removing bias terms (except for the dynamic mixing module) (Chowdhery et al., 2022), applying z-loss regularization (de Brébisson and Vincent, 2016), and disabling dropout. Training is

Model	ARC-c	ARC-e	HellaSwag	OBQA	PIQA	Wino	Avg. Acc	PPL	Params (M)
Base Transformer	30.97	63.38	42.02	33.60	67.30	51.54	48.14	14.79	454
Gated Attention	30.89	64.69	42.73	34.00	67.14	53.35	48.80	14.64	453
ResFormer (Value Residual)	33.62	64.86	43.49	34.40	<b>68.88</b>	52.64	49.65	14.32	454
Naïve Combination (ResFormer+Gate)	32.94	64.52	43.47	32.60	68.34	52.64	49.09	14.25	453
NuResFormer (Internal Anchor)	33.70	65.07	44.23	33.60	68.34	53.12	49.68	14.15	453
ExoFormer (no normalization on anchor)	32.08	63.76	43.49	34.40	<b>68.77</b>	<b>55.64</b>	49.69	14.30	457
Dynamic ExoFormer	33.36	<b>65.87</b>	<b>44.54</b>	34.40	68.28	55.17	<b>50.27</b>	<b>14.09</b>	457
ExoFormer	<b>34.73</b>	64.65	44.28	<b>36.40</b>	67.74	53.59	49.85	14.13	457

Table 1: Performance comparison of model variants on 6 multiple-choice downstream tasks. Reported metrics include accuracy (%), validation loss, perplexity (PPL), and parameter counts. Dynamic ExoFormer achieves the highest overall accuracy and the lowest perplexity, demonstrating the advantages of decoupling the anchor from the first layer and using context-aware mixing. All models use full normalization on anchors unless noted otherwise, and NuResFormer and ExoFormer employ *elementwise* mixing coefficients. A detailed analysis of mixing coefficient granularity is provided in Appendix B.

performed on a 10B-token subset of the FineWeb-Edu dataset (Penedo et al., 2024), which aligns with compute-optimal training as informed by Chinchilla scaling laws (Hoffmann et al., 2022).

We optimize 2D parameters with Muon (specifically the Polar Express variant; Amsel et al. (2025)), applying a cautious weight decay of 0.1 (Chen et al., 2025), while 1D parameters are trained using AdamW without weight decay. Muon was utilized because it represents a state-of-the-art optimizer for large-scale LLM training (Liu et al., 2025). Gradient norms are clipped to 1.0, and all models follow the same optimization setup, to ensure fair comparison across architectures. Training uses a global batch size of 262,144 tokens, a sequence length of 2,048, and a total budget of 10 billion tokens.

We apply linear learning-rate warmup for the first 1,000 steps, with peak learning rates of  $3 \times 10^{-3}$  for AdamW and  $1 \times 10^{-2}$  for Muon. Following warmup, learning rates decay linearly to 10% of their peak values for 20% of the total training steps (Hägle et al., 2024). Full hyperparameters are provided in the Appendix. All experiments are conducted on a single NVIDIA H100 80GB GPU using native BF16 precision, with FlashAttention (Dao et al., 2022) enabled.

**Evaluation Details** We evaluate each benchmark example using a 5-shot prompt. To reduce length-related bias, we report length-normalized accuracy whenever possible. Perplexity is measured on the FineWeb-Edu validation set containing 100 million tokens.

We report results on 6 multiple-choice benchmarks: ARC\_CHALLENGE, ARC\_EASY (Clark et al., 2018), HELASWAG (Zellers et al., 2019), OPENBOOKQA (Mihaylov et al., 2018), PIQA (Bisk et al., 2019), and WINOGRANDE (Sakaguchi et al., 2019).

## 4.2 The Role of Anchor Normalization

As a mild isotropization operator, RMSNorm projects representations onto the unit sphere while preserving directional information and removing scale differences. The unit vector retains the relative alignment between dimensions, which encodes semantic and syntactic features. Second, RMSNorm as a scale-dependent rational function introduces a non-linear transformation into the otherwise linear residual pathway.

This is empirically supported by an analysis of the learned mixing coefficients in unnormalized models. For instance, in the ExoFormer variant without residual normalization, the proportion of near-zero coefficients (below 0.001) for  $\lambda_1$  (the strength of anchor signal) is approximately triple that of the normalized variant. This suppression of the anchor pathway suggests the model is actively compensating for distributional mismatch.

We hypothesize that the naïve combination underperforms for the above reason. When applied to such unbalanced mixtures,  $\sigma(G)$  must compensate for distributional mismatch rather than execute content-aware filtering, resulting in unstable oscillations during training (see Figure 1b) and worse downstream accuracy than ResFormer in isolation.

### 4.3 Extending Mixing to Q, K, and G Pathways

We systematically evaluate the contribution of adding residual pathways for queries ( $Q$ ), keys ( $K$ ), and gating logits ( $G$ ), in addition to the established value ( $V$ ) residual. Table 3 in the Appendix reports the performance of models that residualize different subsets of  $\{Q, K, V, G\}$ , with and without applying RMSNorm to the residual sources.

**The Instability of Unnormalized Q/K Residuals and the Stabilizing Role of QKNorm.** Consistent with prior observations (Zhou et al., 2025), we find a clear hierarchy of stability. Models attempting to use unnormalized Q/K residuals without QKNorm proved impossible to optimize, exhibiting divergent loss in preliminary runs. Critically, adding QKNorm alone stabilizes training and recovers baseline performance. We hypothesize this is because QKNorm compresses the scale of  $Q$  and  $K$ , mitigating the distributional mismatch that arises when injecting early-layer routing signals into deeper layers. Furthermore, adding explicit RMSNorm to the Q/K residual sources on top of QKNorm yields the best results, enabling positive reuse.

**Gating Logit Mixing Is Inherently More Stable.** In contrast to  $Q$  and  $K$ , residual connections for the gating logits  $G$  were straightforward to incorporate even without normalization. We hypothesize that gate logits, which are processed through a sigmoid nonlinearity, are naturally less sensitive to distributional mismatch because the sigmoid compresses their scale.

### 4.4 Mix-Compress-Refine Theory, Gated Attention, and ResFormer

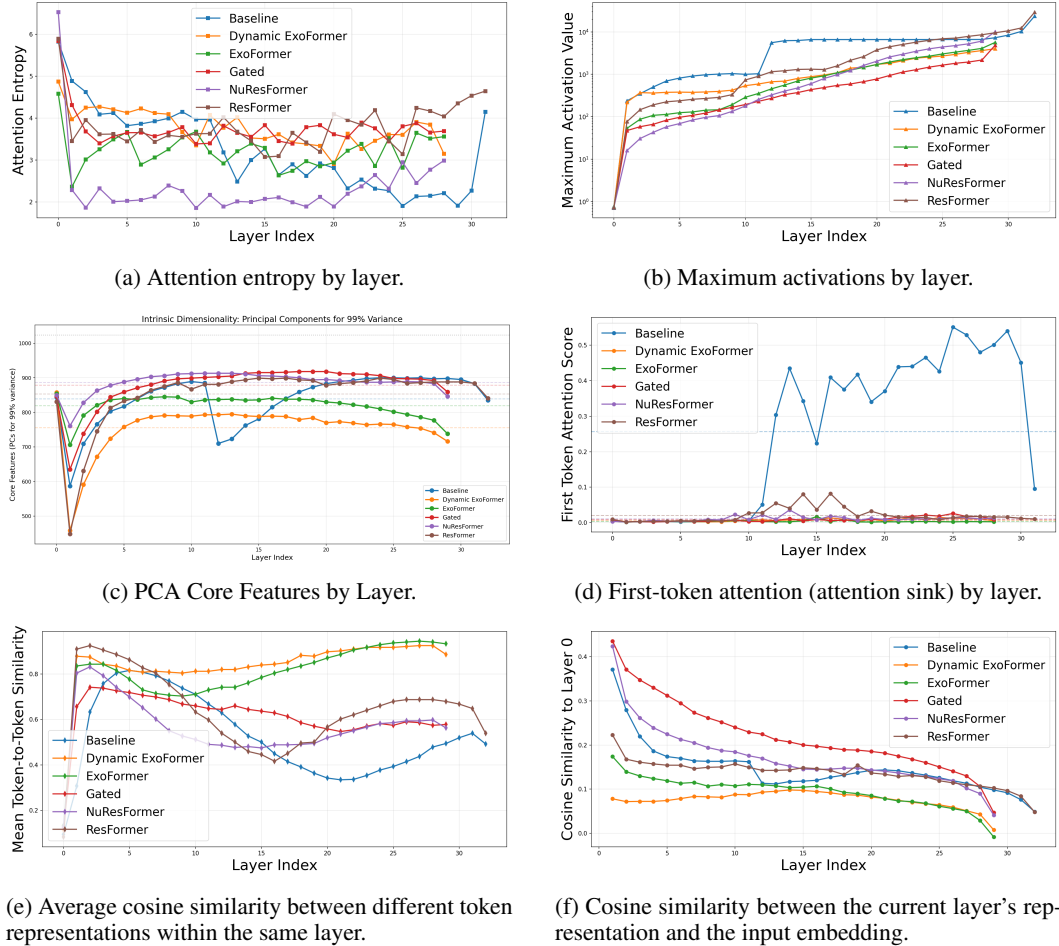


Figure 2: Attention-pattern and representation analysis across model variants. *Elementwise* is used unless stated otherwise. Some graphs include input embeddings for comparison.

As shown in Figure 2, the baseline Transformer’s behavior aligns with the Mix-Compress-Refine theory proposed by de Llano et al. (2025): (1) it begins with a high attention entropy phase for broad, contextual integration of token information, (2) transitions into a compression valley marked by dominant attention sinks that halt mixing and reduce representational dimensionality to filter out useless information, (3) concludes with a sudden rise in attention entropy as sinks dissipate, enabling the refined, token-specific processing necessary for generation.

While these three stages emerge naturally in standard Transformers, they are not optimized for computational efficiency. The model first spends valuable layers collapsing contextual information and then spends more layers slowly building it back up during stage 2 (Figure 2c).

**Gated Attention and residual mixing improve performance by targeting stage 2.** Based on the empirical patterns observed, we propose that the performance gains from gated attention and residual mixing may partly stem from their effect on the model’s second, compression stage.

The gating mechanism appears to address the model’s need to filter irrelevant context, a core function of stage 2. By introducing input-dependent sparsity that selectively modulates information flow at every layer, gated attention seems to provide a form of distributed filtering. This may reduce or eliminate the need for a sharp, dedicated compression phase characterized by dominant attention sinks. The empirical evidence is consistent with this interpretation: as shown in Figure 2c and Table 2, models with gated attention exhibit no clear compression valley and show a drastic reduction in attention sink magnitude compared to the baseline. This suggests the gates could act as a learned, adaptive replacement for the more rigid, sink-based filtering.

Similarly, in models employing residual mixing, the residual pathways may provide an implicit, learned alternative to harsh sink-based filtering. The learned blending could reduce the model’s reliance on extreme, attention-sink-driven compression to isolate useful signals. This is supported by the milder compression valley observed in such models (Figure 2c) and their notable reduction in attention sink magnitude (Table 2).

Metric (Avg)	Baseline	Dynamic ExoFormer	ExoFormer	Gated	NuResFormer	ResFormer
Attention Sink	0.2572	0.0073	<b>0.0041</b>	0.0091	0.0112	0.0212
Token Similarity	<b>0.5365</b>	0.8622	0.8265	0.6328	0.5783	0.6558
PCA Core Features	838.9	752.1	818.3	880.0	<b>887.9</b>	853.8

Table 2: ExoFormer and its dynamic variant exhibit the lowest intrinsic dimensionality (PCA Core Features) and high token similarity, indicative of representation collapse, yet achieve the lowest perplexity and highest downstream accuracy. ExoFormer further eliminates attention sink compared to standard Gated Attention.

#### 4.4.1 The Offloading Hypothesis: Specialization via Exogenous Anchors

We quantify representation collapse using two complementary metrics.

1. **Token Similarity:** Figure 2e plots the average cosine similarity between different token representations within the same layer. While all models exhibit an increase in similarity with depth, ExoFormer is an extreme case, with layer token similarity peaking at 95% and 93% for the dynamic variant. This indicates that, internally, token representations become nearly indistinguishable.
2. **Intrinsic Dimensionality:** As shown in Figure 2c, most models maintain a high intrinsic dimensionality. In stark contrast, ExoFormer’s core features remain consistently below other models, with the final layer utilizing only approximately 738 core features (716 for the dynamic variant), compared to 835 for the baseline.

We note that residual normalizations are unlikely to be responsible for this over-smoothing, given that NuResFormer, employing full residual norms, yields the greatest mean of PCA core features, while E-ExoFormer (no norm) displays similar signs of collapse.

Furthermore, analyzing the trajectory of hidden states reveals a striking divergence from the starting point. Figure 2f shows the cosine similarity between each layer’s representation and that of the input

embedding. In ExoFormer, this similarity starts extremely low and steadily decays, with deeper layers becoming nearly orthogonal or even slightly anti-correlated with the initial representation.

**The “Offloading” Hypothesis** Standard theory posits that over-smoothing degrades model performance, as it implies a loss of information necessary for prediction. The fact that dynamic E-ExoFormer achieves the **highest average accuracy (50.27%)** and **lowest perplexity (14.09)** while exhibiting internal smoothing—near-identical token representations and low intrinsic dimensionality—presents a clear contradiction.

To resolve this paradox, we propose the **Offloading Hypothesis**: the exogenous anchor allows the sequential layers to specialize almost exclusively in the final “refinement” stage (Stage 3) of the Mix-Compress-Refine cycle. Evidence for this specialization is visible in the token-similarity trajectory (Figure 2e). All models show a pattern where similarity rises to an early maximum, dips to a local minimum, rises again, and finally falls in the last layer. We interpret the local minimum as the start of Stage 3: the refinement phase dedicated to preparing representations for next-token prediction. Notably, ExoFormer variants spend approximately two-thirds of their layers in this stage, the highest proportion of any model, while the baseline spends only one-third.

This specialization is possible because exogenous anchors fundamentally change how information is managed. In a standard Transformer, the residual stream must concurrently carry two critical types of information: (1) distinct features that preserve token identity (“What token am I?”), and (2) transformed, task-relevant features that evolve through the layers to support next-token prediction. Over-smoothing in a standard model catastrophically loses the first type, crippling the model’s ability to route information. ExoFormer circumvents this by introducing a permanent reference library, the exogenous anchor, that is re-injected at every layer.

This architecture enables a form of **functional offloading** that separates these concerns:

1. **The Anchor assumes the “Identity” role.** By providing a guaranteed, high-fidelity source of token distinctiveness at every layer, the exogenous anchor relieves the main residual stream from the duty of preserving static token features. The dedicated anchor parameters ( $W_{\text{anc}}^Q, W_{\text{anc}}^K, W_{\text{anc}}^V, W_{\text{anc}}^G$ ) can specialize exclusively in maximizing variance and distinctiveness.
2. **The Sequential Layers specialize in “Computation.”** With identity information externally supplied, the internal layers are liberated from the constraint of preserving early-layer geometry. The observed “collapse” can thus be reinterpreted as a gradual signal purification. The layers act as aggressive filters, compressing the representation to focus solely on the progressive, step-by-step computation required for reasoning, while dynamically discarding redundant or static information.

This clean separation allows each component to excel at its specialized function, directly causing the observed extremes: maximal internal smoothing and minimal similarity to the first layer. Further analysis is warranted to fully characterize the dynamics of this smoothing effect and its precise relationship to performance, but the evidence suggests that ExoFormer’s “collapse” is a feature of its architecture.

## 5 Conclusion

We introduce NuResFormer, a framework enabling normalized cross-layer residual mixing across all attention pathways, and identify the architectural tension when the first layer must serve as both a reusable anchor and a progressive computational block. To resolve this, we propose ExoFormer, which learns dedicated exogenous anchor projections, decoupling these roles and consistently outperforming NuResFormer variants. We connect these improvements to the Mix-Compress-Refine theory and propose the offloading hypothesis: external anchors preserve token identity, allowing internal layers to specialize in refinement, which explains ExoFormer’s superior efficiency and performance despite signs of internal representation collapse.

## 6 Limitations

The experiments were conducted at a modest scale (450M parameters, 10B tokens), and the observed behaviors may not generalize to larger models or longer training. Due to resource constraints, we did not perform an exhaustive search for the optimal initialization of the coefficient  $\lambda$ . The evaluation focuses on multiple-choice benchmarks, leaving the impact on long-context tasks unknown. Finally, while the results are empirically grounded, a formal theoretical explanation for why normalized reuse works is still lacking.

## References

Noah Amsel, David Persson, Christopher Musco, and Robert M. Gower. 2025. The polar express: Optimal matrix sign methods and their application to the muon algorithm. *Preprint*, arXiv:2505.16932.

Yonatan Bisk, Rowan Zellers, Ronan Le Bras, Jianfeng Gao, and Yejin Choi. 2019. Piqa: Reasoning about physical commonsense in natural language. *Preprint*, arXiv:1911.11641.

Lizhang Chen, Jonathan Li, Kaizhao Liang, Baiyu Su, Cong Xie, Nuo Wang Pierse, Chen Liang, Ni Lao, and Qiang Liu. 2025. Cautious weight decay. *Preprint*, arXiv:2510.12402.

Aakanksha Chowdhery, Sharan Narang, Jacob Devlin, Maarten Bosma, Gaurav Mishra, Adam Roberts, Paul Barham, Hyung Won Chung, Charles Sutton, Sebastian Gehrmann, Parker Schuh, Kensen Shi, Sasha Tsvyashchenko, Joshua Maynez, Abhishek Rao, Parker Barnes, Yi Tay, Noam Shazeer, Vinodkumar Prabhakaran, Emily Reif, Nan Du, Ben Hutchinson, Reiner Pope, James Bradbury, Jacob Austin, Michael Isard, Guy Gur-Ari, Pengcheng Yin, Toju Duke, Anselm Levskaya, Sanjay Ghemawat, Sunipa Dev, Henryk Michalewski, Xavier Garcia, Vedant Misra, Kevin Robinson, Liam Fedus, Denny Zhou, Daphne Ippolito, David Luan, Hyeontaek Lim, Barret Zoph, Alexander Spiridonov, Ryan Sepassi, David Dohan, Shivanii Agrawal, Mark Omernick, Andrew M. Dai, Thanumalayan Sankaranarayana Pillai, Marie Pellat, Aitor Lewkowycz, Erica Moreira, Rewon Child, Oleksandr Polozov, Katherine Lee, Zongwei Zhou, Xuezhi Wang, Brennan Saeta, Mark Diaz, Orhan Firat, Michele Catasta, Jason Wei, Kathy Meier-Hellstern, Douglas Eck, Jeff Dean, Slav Petrov, and Noah Fiedel. 2022. Palm: Scaling language modeling with pathways. *Preprint*, arXiv:2204.02311.

Peter Clark, Isaac Cowhey, Oren Etzioni, Tushar Khot, Ashish Sabharwal, Carissa Schoenick, and Oyvind Tafjord. 2018. Think you have solved question answering? try arc, the ai2 reasoning challenge. *Preprint*, arXiv:1803.05457.

Tri Dao, Daniel Y. Fu, Stefano Ermon, Atri Rudra, and Christopher Ré. 2022. Flashattention: Fast and memory-efficient exact attention with io-awareness. *Preprint*, arXiv:2205.14135.

Alexandre de Brébisson and Pascal Vincent. 2016. The z-loss: a shift and scale invariant classification loss belonging to the spherical family. *Preprint*, arXiv:1604.08859.

Enrique Queipo de Llano, Álvaro Arroyo, Federico Barbero, Xiaowen Dong, Michael Bronstein, Yann LeCun, and Ravid Shwartz-Ziv. 2025. Attention sinks and compression valleys in llms are two sides of the same coin. *Preprint*, arXiv:2510.06477.

Alex Henry, Prudhvi Raj Dachapally, Shubham Pawar, and Yuxuan Chen. 2020. Query-key normalization for transformers. *Preprint*, arXiv:2010.04245.

Jordan Hoffmann, Sebastian Borgeaud, Arthur Mensch, Elena Buchatskaya, Trevor Cai, Eliza Rutherford, Diego de Las Casas, Lisa Anne Hendricks, Johannes Welbl, Aidan Clark, Tom Hennigan, Eric Noland, Katie Millican, George van den Driessche, Bogdan Damoc, Aurelia Guy, Simon Osindero, Karen Simonyan, Erich Elsen, Jack W. Rae, Oriol Vinyals, and Laurent Sifre. 2022. Training compute-optimal large language models. *Preprint*, arXiv:2203.15556.

Alexander Hägele, Elie Bakouch, Atli Kosson, Loubna Ben Allal, Leandro Von Werra, and Martin Jaggi. 2024. Scaling laws and compute-optimal training beyond fixed training durations. *Preprint*, arXiv:2405.18392.

Jingyuan Liu, Jianlin Su, Xingcheng Yao, Zhejun Jiang, Guokun Lai, Yulun Du, Yidao Qin, Weixin Xu, Enzhe Lu, Junjie Yan, Yanru Chen, Huabin Zheng, Yibo Liu, Shaowei Liu, Bohong Yin, Weiran He, Han Zhu, Yuzhi Wang, Jianzhou Wang, Mengnan Dong, Zheng Zhang, Yongsheng Kang, Hao Zhang, Xinran Xu, Yutao Zhang, Yuxin Wu, Xinyu Zhou, and Zhilin Yang. 2025. Muon is scalable for llm training. *Preprint*, arXiv:2502.16982.

Todor Mihaylov, Peter Clark, Tushar Khot, and Ashish Sabharwal. 2018. Can a suit of armor conduct electricity? a new dataset for open book question answering. *Preprint*, arXiv:1809.02789.

Guilherme Penedo, Hynek Kydlíček, Loubna Ben allal, Anton Lozhkov, Margaret Mitchell, Colin Raffel, Leandro Von Werra, and Thomas Wolf. 2024. The fineweb datasets: Decanting the web for the finest text data at scale. *Preprint*, arXiv:2406.17557.

Zihan Qiu, Zekun Wang, Bo Zheng, Zeyu Huang, Kaiyue Wen, Songlin Yang, Rui Men, Le Yu, Fei Huang, Suozhi Huang, Dayiheng Liu, Jingren Zhou, and Junyang Lin. 2025. Gated attention for large language models: Non-linearity, sparsity, and attention-sink-free. *Preprint*, arXiv:2505.06708.

Keisuke Sakaguchi, Ronan Le Bras, Chandra Bhagavatula, and Yejin Choi. 2019. Winogrande: An adversarial winograd schema challenge at scale. *Preprint*, arXiv:1907.10641.

Noam Shazeer. 2020. Glu variants improve transformer. *Preprint*, arXiv:2002.05202.

Han Shi, Jiahui Gao, Hang Xu, Xiaodan Liang, Zhenguo Li, Lingpeng Kong, Stephen Lee, and James T Kwok. 2022. Revisiting over-smoothing in bert from the perspective of graph. *arXiv preprint arXiv:2202.08625*.

Jianlin Su, Yu Lu, Shengfeng Pan, Ahmed Murtadha, Bo Wen, and Yunfeng Liu. 2023. Roformer: Enhanced transformer with rotary position embedding. *Preprint*, arXiv:2104.09864.

Ashish Vaswani, Noam Shazeer, Niki Parmar, Jakob Uszkoreit, Llion Jones, Aidan N Gomez, Łukasz Kaiser, and Illia Polosukhin. 2017. Attention is all you need. *Advances in Neural Information Processing Systems*, 30.

Elena Voita, David Talbot, Fedor Moiseev, Rico Sennrich, and Ivan Titov. 2019. Analyzing multi-head self-attention: Specialized heads do the heavy lifting, the rest can be pruned. *Preprint*, arXiv:1905.09418.

Da Xiao, Qingye Meng, Shengping Li, and Xingyuan Yuan. 2025. Muddformer: Breaking residual bottlenecks in transformers via multiway dynamic dense connections. *Preprint*, arXiv:2502.12170.

Zhenda Xie, Yixuan Wei, Huanqi Cao, Chenggang Zhao, Chengqi Deng, Jiashi Li, Damai Dai, Huazuo Gao, Jiang Chang, Kuai Yu, Liang Zhao, Shangyan Zhou, Zhean Xu, Zhengyan Zhang, Wangding Zeng, Shengding Hu, Yuqing Wang, Jingyang Yuan, Lean Wang, and Wenfeng Liang. 2026. mhc: Manifold-constrained hyper-connections. *Preprint*, arXiv:2512.24880.

Greg Yang, Edward J. Hu, Igor Babuschkin, Szymon Sidor, Xiaodong Liu, David Farhi, Nick Ryder, Jakub Pachocki, Weizhu Chen, and Jianfeng Gao. 2022. Tensor programs v: Tuning large neural networks via zero-shot hyperparameter transfer. *Preprint*, arXiv:2203.03466.

Rowan Zellers, Ari Holtzman, Yonatan Bisk, Ali Farhadi, and Yejin Choi. 2019. Hellaswag: Can a machine really finish your sentence? *Preprint*, arXiv:1905.07830.

Daquan Zhou, Bingyi Kang, Xiaojie Jin, Linjie Yang, Xiaochen Lian, Zihang Jiang, Qibin Hou, and Jiashi Feng. 2021. Deepvit: Towards deeper vision transformer. *arXiv preprint arXiv:2103.11886*.

Zhanchao Zhou, Tianyi Wu, Zhiyun Jiang, Fares Obeid, and Zhenzhong Lan. 2025. Value residual learning. *Preprint*, arXiv:2410.17897.

Defa Zhu, Hongzhi Huang, Zihao Huang, Yutao Zeng, Yunyao Mao, Banggu Wu, Qiyang Min, and Xun Zhou. 2025. Hyper-connections. *Preprint*, arXiv:2409.19606.

## A Complete Evaluation Results

Model	ARC-c	ARC-e	HellaSwag	OBQA	PIQA	Wino	Avg. Acc	PPL	Params (M)
<b>Baselines</b>									
Base Transformer	30.97	63.38	42.02	33.60	67.30	51.54	48.14	14.79	454
Gated Attention	30.89	64.69	42.73	34.00	67.14	53.35	48.80	14.64	453
ResFormer (Value Residual)	33.62	64.86	43.49	34.40	<b>68.88</b>	52.64	49.65	14.32	454
Naïve Combination (ResFormer+Gate)	32.94	64.52	43.47	32.60	68.34	52.64	49.09	14.25	453
<b>NuResFormer Variants (Internal Anchor)</b>									
E-NuResFormer (only Q/K residual norms)	31.74	64.27	43.83	33.00	68.23	52.41	48.91	14.21	453
H-NuResFormer (only Q/K residual norms)	<b>34.73</b>	64.06	44.45	34.20	67.57	53.04	49.68	14.21	453
S-NuResFormer (only Q/K residual norms)	32.85	<b>66.08</b>	43.87	34.20	68.28	53.67	49.83	14.22	453
E-NuResFormer (no norm, {V,G} only)	32.42	64.94	43.80	35.00	67.52	51.54	49.20	14.24	453
H-NuResFormer (no norm, {V,G} only)	31.23	64.18	43.50	34.00	67.68	54.06	49.11	14.22	453
S-NuResFormer (no norm, {V,G} only)	31.83	64.44	43.66	34.80	68.44	52.49	49.28	14.24	453
E-NuResFormer (full)	33.70	65.07	44.23	33.60	68.34	53.12	49.68	14.15	453
H-NuResFormer (full)	33.79	65.11	44.09	33.40	67.41	52.72	49.42	14.17	453
S-NuResFormer (full)	32.42	64.02	43.93	33.20	67.90	53.20	49.11	14.17	453
<b>ExoFormer Variants (External Anchor)</b>									
E-ExoFormer (no norm)	32.08	63.76	43.49	34.40	68.77	<b>55.64</b>	49.69	14.30	457
<b>Dynamic E-ExoFormer</b>	33.36	65.87	<b>44.54</b>	34.40	68.28	55.17	<b>50.27</b>	<b>14.09</b>	457
E-ExoFormer (full)	<b>34.73</b>	64.65	44.28	<b>36.40</b>	67.74	53.59	49.85	14.13	457
H-ExoFormer (full)	32.17	65.87	44.00	32.40	68.23	54.06	49.23	14.14	457
S-ExoFormer (full)	32.17	65.66	44.33	33.60	68.06	51.14	49.16	14.15	457

Table 3: Comprehensive evaluation results on 6 multiple-choice downstream tasks (accuracy in %), validation perplexity (PPL), and parameter counts. Dynamic E-ExoFormer achieves the highest overall accuracy and lowest perplexity. Full residual norms are utilized unless specified otherwise. “no norm” indicates no residual normalization was applied to the anchor signal. Bold values indicate the best performance for each metric.

## B Residual Mixing Granularity and Emergent Head-level Structure

A central design choice in our unified residual framework is the granularity at which mixing coefficients  $\lambda$  are learned. We evaluate three levels—scalar (S), headwise (H), and elementwise (E)—across both NuResFormer and ExoFormer variants.

**Granularity in NuResFormer.** Among NuResFormer configurations, scalar mixing achieves the highest average downstream accuracy (49.83%) despite having the fewest parameters. Headwise mixing performs nearly as well (49.68% to 49.42%), indicating that allocating one degree of freedom per attention head captures a significant portion of the beneficial structure. Elementwise mixing yields the best language modeling perplexity (14.15 under full residual norms) but slightly lower downstream accuracy than its scalar counterpart. This suggests increased parametric freedom can improve in-distribution loss but may not generalize as well.

**Granularity in ExoFormer.** ExoFormer exhibits a notably different profile. Here, elementwise mixing (E-ExoFormer) achieves the overall best performance, attaining the highest average accuracy (49.85%) and the lowest validation perplexity (14.13) of any static model. This reversal indicates that the effectiveness of coefficient granularity is architecture-dependent. We hypothesize that in this cleaner setting (due to decoupling), the optimizer can effectively exploit fine-grained mixing to orchestrate precise reuse policies without compromising generalization.

**Emergent Head Structure in Elementwise Mixing.** A striking qualitative finding emerges from visualizing the learned elementwise coefficients, as shown in Figure 3. For the value pathway ( $V$ ), the heatmaps exhibit *sharp boundaries that align precisely with head blocks*. Within each head—a contiguous span of  $d_k$  channels—the mixing coefficients  $\lambda_{n,1}^V$  and  $\lambda_{n,2}^V$  are nearly constant, with primary discontinuities occurring *between heads*. This structure emerges despite the optimizer having

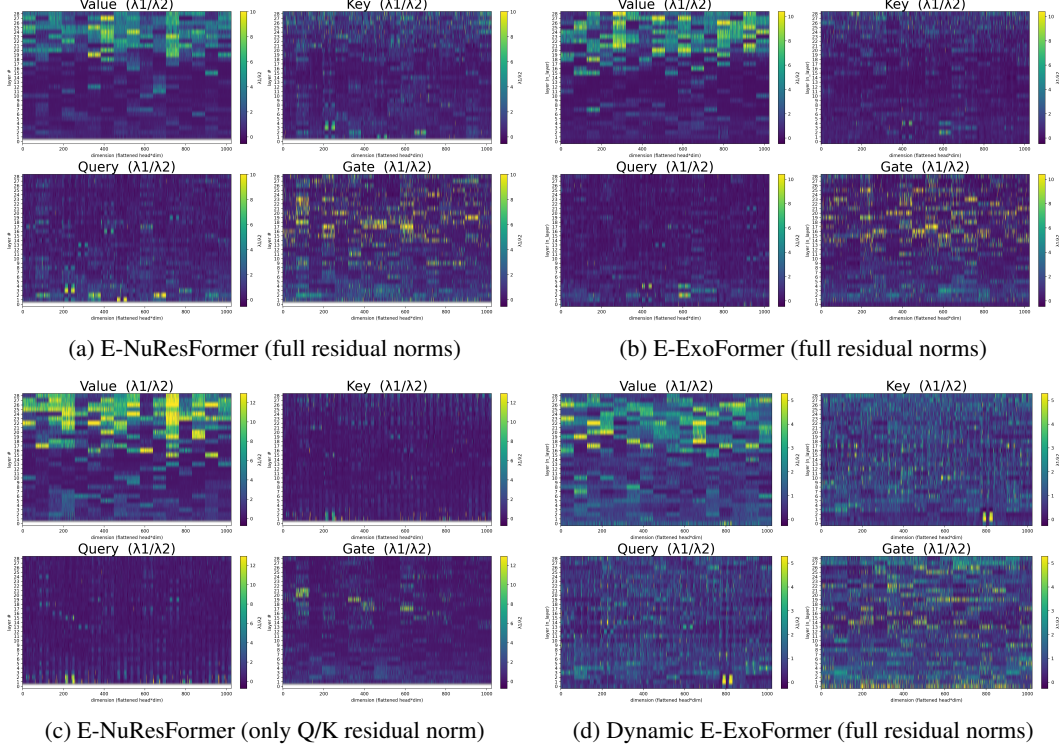


Figure 3: Heatmaps showing the learned mixing coefficient ratio  $\lambda_{n,1}/\lambda_{n,2}$  for each residualized component  $\{Q, K, V, G\}$  across layers (y-axis) and channels/heads (x-axis). This ratio quantifies the model’s reliance on the anchor relative to the current layer’s projection; a higher value indicates stronger reuse of the early signal. Even with elementwise freedom, the learned pattern is largely constant within heads for  $V$ , while  $Q$ ,  $K$ , and  $G$  exhibit finer-grained structure. The dynamic variant shows more uniform distributions across channels and layers.

the freedom to set each channel independently. The result implies that the natural, discovered unit of residual control for content ( $V$ ) is the attention head as a whole, aligning with previous research on heads as specialized submodules for routing information (Voita et al., 2019).

The patterns for queries ( $Q$ ), keys ( $K$ ), and gate logits ( $G$ ) are markedly different. These components frequently exhibit *finer-grained, intra-head structure*, such as alternating bands of high and low reuse (“striping”). This suggests a form of sub-head specialization, where specific channel subspaces within a head are selectively reused or suppressed. Notably, the positions of these high/low bands in  $Q$  often align with those in  $K$ .

**Flexibility Enabled by Dynamic Mixing.** As shown in Figure 3d,  $\lambda_{n,1}/\lambda_{n,2}$  for queries, keys, and gating logits are substantially more uniformly distributed across channels and layers in the dynamic variant, with fewer banded structures seen in static mixing. Rather than converging to a fixed, layer-specific reuse policy, the model can modulate the strength of the anchor pathway for each component in real time based on the input sequence. This flexibility is particularly beneficial for the routing ( $Q$ ,  $K$ ) and selection ( $G$ ) components, whose optimal mixing strategy may depend heavily on immediate contextual needs.

## C Mixing Coefficient

Figure 4 shows the layer-wise evolution of the mixing coefficient ratio  $\lambda_{n,1}/\lambda_{n,2}$  for each attention component.

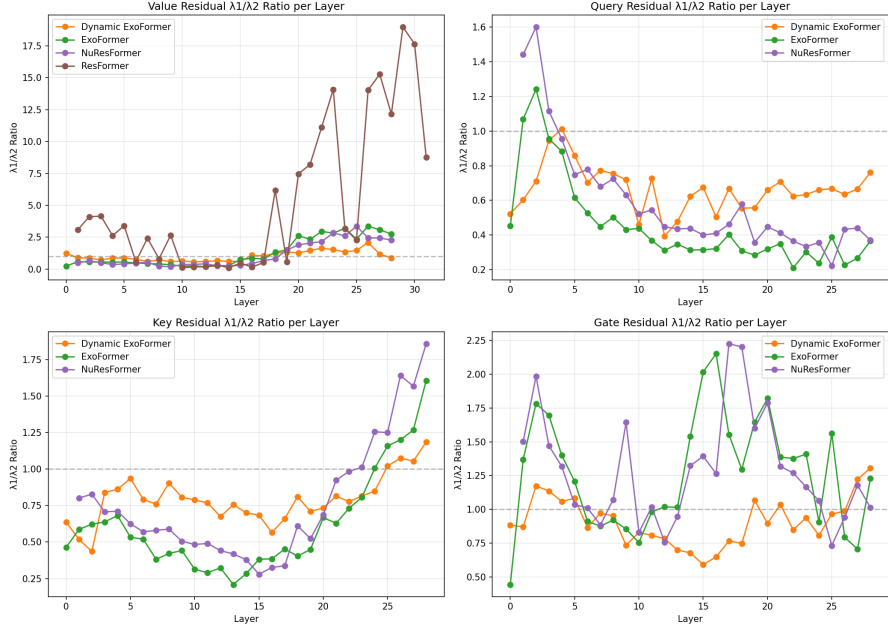


Figure 4: The ratio  $\lambda_{n,1}/\lambda_{n,2}$  plotted for each component ( $Q, K, V, G$ ) across layers for models using *elementwise* mixing. Values greater than 1 indicate stronger reliance on the anchor signal, while values less than 1 indicate preference for current-layer projections.

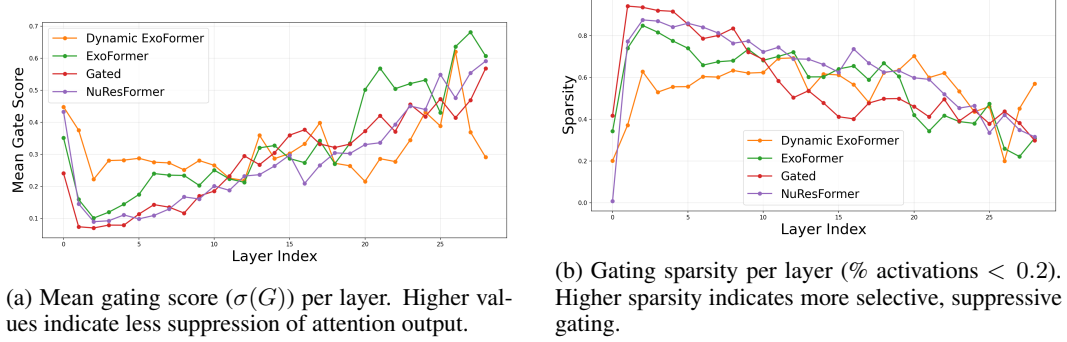


Figure 5: Depth-wise analysis of gating behavior across model variants.

## D Gate Activation Profiles and First-Layer Selectivity

NuResFormer’s first layer exhibits a **high mean gate activation** (approximately 0.4-0.5), indicating its gating mechanism is not highly suppressive, allowing roughly half of the attention output to pass through. This contrasts sharply with standalone Gated Attention, where the first-layer mean activation is significantly lower (approximately 0.2). Following this initial peak, gate activations fall rapidly in intermediate layers before rising steadily again in deeper layers.

This pattern provides direct empirical support for the architectural tension hypothesized in Section 3.5. When the first layer also serves as the residual anchor (as in NuResFormer), it faces conflicting objectives: its gate logits  $G_1$  must perform effective, context-dependent selection for the first layer’s own computation while also producing a reusable anchor signal  $G_{\text{anc}}$  for all subsequent layers. The high first-layer gate activation suggests a resolution: the layer adopts a permissive gating policy to ensure the anchor gate logits retain broad, generally useful information, sacrificing some first-layer selectivity in the process.

ExoFormer exhibits an attenuated version of the same profile (Figure 5a); its first-layer activation is elevated compared to standalone gating but lower than NuResFormer’s. As shown in Figure 5b,

offloading the anchor role allows ExoFormer to partially restore the first layer’s capacity for selective gating, achieving intermediate sparsity levels between NuResFormer and standalone Gated Attention.

## E Hidden State Similarity

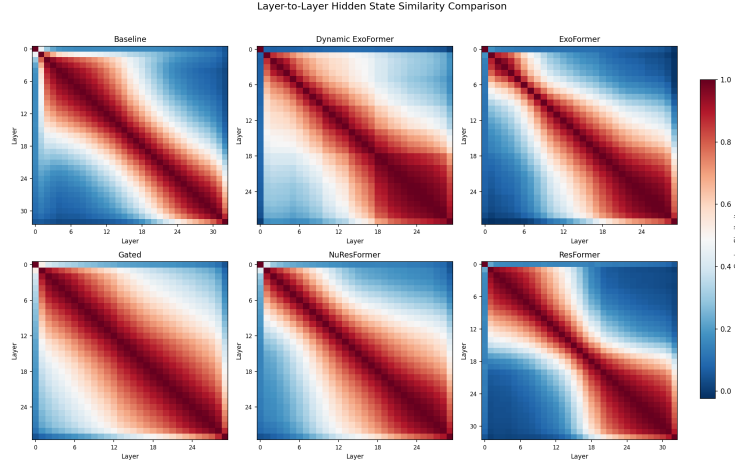


Figure 6: Pairwise cosine similarity of hidden states across transformer layers for models using *elementwise* mixing. Brighter colors indicate higher similarity.

## F Hyperparameters

Hyperparameter	No Gate	With Gate	Decoupled (ExoFormer)
Parameters (M)	454	453	457
Layers	32	29	29
Attention Heads		16	
Hidden Dimension		1024	
FFN Dimension		4096	
Tie Word Embedding		False	
Vocabulary Size		57,601	
Activation Function		SwiGLU	
Position Embedding		RoPE ( $\theta = 500,000$ )	
Sequence Length		2048	
Batch Size (tokens)		262,144	
Training Tokens		10B	
Warmup Steps		1000	
Warmdown Steps		7630 (20%)	
Total Steps		38,147	

### Optimization

Optimizer	Muon + AdamW
Muon Learning Rate	0.01
AdamW Learning Rate	0.003
Learning Rate Schedule	Linear
Adam $\beta$	(0.9, 0.95)
Muon Momentum	0.95
Gradient Clip	1.0
Dropout	0.0
Cautious Weight Decay	True
Muon Weight Decay	0.1
AdamW Weight Decay	0.0
Z Loss Weight	1e-5
RMSNorm Epsilon	1e-6
QK Normalization	True

Table 4: Training hyperparameters for models with different configurations. Layer depth was reduced for gated variants to maintain comparable parameter counts. All models were trained on 10B tokens from the FineWeb-Edu dataset.